Journal of Materials Chemistry B

ROYAL SOCIETY OF CHEMISTRY

PAPER

View Article Online
View Journal | View Issue

Cite this: J. Mater. Chem. B, 2025, 13, 12134

Insulin-producing INS-1 cell cultures on biomimetic 3D scaffolds

Mikhail Parker,[a] Nataraja Sekhar Yadavalli, *[c] Kristina Peranidze, [ab] Eugene Boland,[c] Vladimir Reukov[b] and Sergiy Minko *[a]

Three-dimensional cell cultures on biomimetic scaffolds have gained significant attention in tissue engineering, drug delivery, and scalable cell production. Current challenges in creating an ideal scaffold are providing maximum space for cells to grow while ensuring efficient nutrient, metabolite, and gas exchange to prevent the formation of necrotic or apoptotic regions. In our work, we grow insulin-producing INS-1 cells on touch-spun polycaprolactone (PCL) fiber scaffolds. Touch-spinning allows the creation of finely aligned 3D mesh-like fiber scaffolds with controllable distance between the fibers, resulting in a minimum of abiotic scaffold material and providing maximum space for cells to grow. Adding Matrigel at different combinations allowed us to control the INS-1 proliferation profile and grow them either in the form of scarce large (up to 1 mm) spheroids (no Matrigel), numerous smaller (about 150–200 μm in diameter) spheroids (Matrigel added to the cells only) or cell sheets (Matrigel added to both cells and fibers). Growing INS-1 cells as nanofiber-reinforced cell sheets is of utmost importance because it opens the possibility of using them in cell sheet tissue engineering. Obtaining free-floating sheets of insulin-producing cells by traditional means is typically challenging due to their fragility. Being only about 4–6 cells thick, INS-1 cell sheets are not prone to forming necrotic cores, which is a common problem for all 3D spheroid cultures when they reach a diameter of more than 150–200 μm. At the same time, they preserved their insulin production ability and characteristics of 3D cultures, such as numerous cell-to-cell contacts and metabolic activity.

Received 8th March 2025,
Accepted 10th August 2025

DOI: 10.1039/d5tb00519a

rsc.li/materials-b

1. Introduction

Type 1 diabetes (T1D) is a chronic condition primarily caused by the autoimmune destruction of insulin-producing β-cells in the pancreas, leading to an inability to produce insulin and thus requiring exogenous insulin administration for survival. The burden of T1D is substantial and growing; in 2021, approximately 84 million individuals worldwide lived with T1D.[1] The only clinically approved method for cell replacement therapy of T1D is the Edmonton protocol, during which donor pancreatic islets are lodged into the liver's portal vein, enabling direct insulin secretion into the bloodstream.[2] This technique requires immunosuppressants to prevent allograft rejection and protect β-cells from the immune system.[3–6] However, immune suppression has multiple side effects, and application of the Edmonton protocol is limited when using insulin-producing cells derived from alternative sources, such as induced pluripotent stem cells (iPSCs) and embryonic stem cells (ESCs), due to increased risks of tumorigenicity and strong immune reactions.[7–11]

An alternative approach involves growing these cells within specialized scaffolds that can be transplanted subcutaneously.[12,13] This method allows for the easy removal of the constructs if tumor formation or acute immune reactions occur. Some scaffolds can also be modified to act as a physical barrier, thus reducing the need for immunosuppressive treatments.[5,14] Furthermore, the use of scaffolds offers ease of surgical manipulation and improves the viability and functionality of the transplanted cells, as detailed in studies on scaffold-based immunological modulation.[15]

Besides clinical applications, three-dimensional constructs can be instrumental in *in vitro* research and drug testing. For example, due to their 3D structure, spheroid culture systems have significantly more cell-to-cell contacts than in 2D cultures, thus better mimicking their natural tissue environments. This can improve the reliability of preclinical drug screening, thereby potentially leading to better therapeutic outcomes.[16–21]

There are several different types of scaffolds for cell seeding, which can be divided into subcategories based on their consistency, material, and manufacturing process. Based on consistency, scaffolds can be "soft" and "hard". Soft scaffolds are usually made

[a] Nanostructured Materials Laboratory, University of Georgia, Athens, GA, 30602, USA. E-mail: sminko@uga.edu
[b] Department of Textiles, Merchandising and Interiors, University of Georgia, Athens, GA, 30602, USA
[c] CytoNest, Inc., 425 River Road, Athens, GA, 30602, USA. E-mail: natarajasy@cytonest.com

Table 1 Advantages of touch-spun fibrous scaffolds (3DTSS)

Other methods	Advantages of 3DTSS
Hydrogel	Mechanical strength, long-term stability, scaffold structure control, adaptable for cell sheet tissue engineering
Decellularized tissues	High porosity, scaffold structure control, cost-efficient, simple fabrication
3D printed porous scaffolds	High porosity, low volume fraction of abiotic materials, resorbability control
Electrospun fibrous scaffolds	Scaffold structure control

in the form of hydrogels. They can be manufactured from materials that are natural to the body, like polysaccharides (agar, chitosan, hyaluronic acid, pectins, alginate *etc.*) and proteins (collagen, fibrin *etc.*); biocompatible synthetic materials (polyethylene glycol (PEG), polyvinyl alcohol (PVA), and polyacrylic acid (PAA)); and combinations of natural and synthetic materials.[22,23] "Hard" scaffolds can be divided into manufactured and tissue-based, made from decellularized tissues.[24] Manufactured scaffolds could be made by means of 3D printing or electrospinning from biocompatible synthetic materials, such as polycaprolactone (PCL), and a combination of synthetic and natural materials (*e.g.*, pectin–chitosan–PVA nanofibers).[25] Each scaffold type has its pros and cons (Table 1).

The hydrogels used for cell culture are physically (hydrogen bonds) crosslinked polymer (natural or synthetic) chains. The hydrogels are highly porous materials, but the pore or mesh size is much smaller than the cell size. Cells proliferate by disrupting a weak hydrogel structure. Thick hydrogels might impede nutrients and gas exchange, affecting organoid growth.[26] Other disadvantages of using hydrogels as scaffolds include limited mechanical strength, lack of long-term stability, and limited control over their structure.[27] Recellularization of previously decellularized tissues is a time-consuming, complicated process that requires donor tissue and expensive equipment. Synthetic material-based scaffolds have much better mechanical strength and are easy and inexpensive to fabricate (Table 1).[28] However, such scaffolds do not perfectly imitate the natural tissue environment as decellularized tissues, although fibrous scaffolds come closer to natural structures.[29]

Fibrous scaffolds are usually fabricated using a technique known as electrospinning. Main disadvantages of this method are the inability to have precise control over distances between fibers and limited control in achieving complex 3D structures. As a result, the scaffold abiotic material can occupy a substantial portion of the construct's mass, thus limiting the space available for cellular growth. It should be noted that excess of abiotic material remains a prevalent challenge with many manufactured cells-on-scaffold systems. This concern is particularly critical for insulin-producing cell (IPC) systems, as normoglycemia in humans is maintained by approximately one billion β-cells or about 1 gram of tissue weight.[30,31] Consequently, optimizing the occupancy of IPCs on scaffolds is a primary concern to maximize therapeutic efficacy. Another significant issue, especially relevant for large cell clusters, is the formation of a necrotic core due to insufficient nutrient and oxygen transport to cells in the center of the construct. Research indicates that necrotic core formation typically occurs in cell clusters exceeding 150–200 μm in thickness, as cells can only efficiently exchange nutrients from blood vessels across a distance of approximately 200 μm.[32,33] This necessitates innovative design adaptations in 3D tissue engineering to ensure adequate cellular viability and function throughout the construct.

Considering the factors discussed above, an ideal scaffold for cultivating IPCs for transplantation and drug testing should optimize cellular surface area while minimizing material use and structural gaps. It is crucial that the cell sheets or spheroids maintain a thickness or diameter of no more than ~200 μm per layer within the total scaffold construct to prevent the formation of necrotic cores. Furthermore, the design should enhance cell-to-cell interactions, effectively replicating the natural cellular environment found in the body.

To achieve these scaffold characteristics, we cultured an insulin-producing cell line derived from rat insulinoma (INS-1)[18,34–36] on innovative touch-spun three-dimensional scaffolds (3DTSS),[37,38] both with and without the inclusion of Matrigel—a mouse tumor extract comprising natural extracellular matrix (ECM) components. Touch-spinning is a novel technique that enables the creation of highly organized 3D fibrous scaffolds featuring controlled fiber spacing (Fig. 1(C), 2(C), Fig. 3, and Fig. S1). In this study, the scaffolds were constructed using crisscrossed fibers with diameters ranging from 1 to 3 μm, arranged in a rectangular or square grid pattern with 90-degree angles and 40–100 μm spacing between fibers, achieving porosity levels exceeding 90%, which minimizes the use of scaffolding biomaterials as shown in Fig. 1(A)–(C). After alignment into the form of the grid, these fibers could be fused together by high temperature, thus creating a firm and robust structure. This is especially important for thin one-layered scaffolds because after seeding, cells start to proliferate and migrate, often pulling on their nanofibers, which causes misalignment of fibers and the creation of "holes" in the cell sheet. Fiber-fusion prevents this problem (Fig. S2(B) and (C)).

These scaffolds supported the formation of diverse cellular structures, from spheroid-like to sheet-like configurations, when seeded with INS-1 cells (Fig. 1(D)–(G)). The variety in construct formation and cell behavior was influenced by the 3D fiber arrangement and the application of Matrigel, demonstrating the scaffold's capability to mimic natural tissue environments through its design and composition.

2. Materials and methods

Dulbecco's modified Eagle's medium (DMEM) (Cat. No. D6429), RPMI-1640 (Cat. No. R0883), fetal bovine serum (FBS) (Cat. No. ES-009-B), L-glutamine (Cat. No. TMS-002-C), sodium

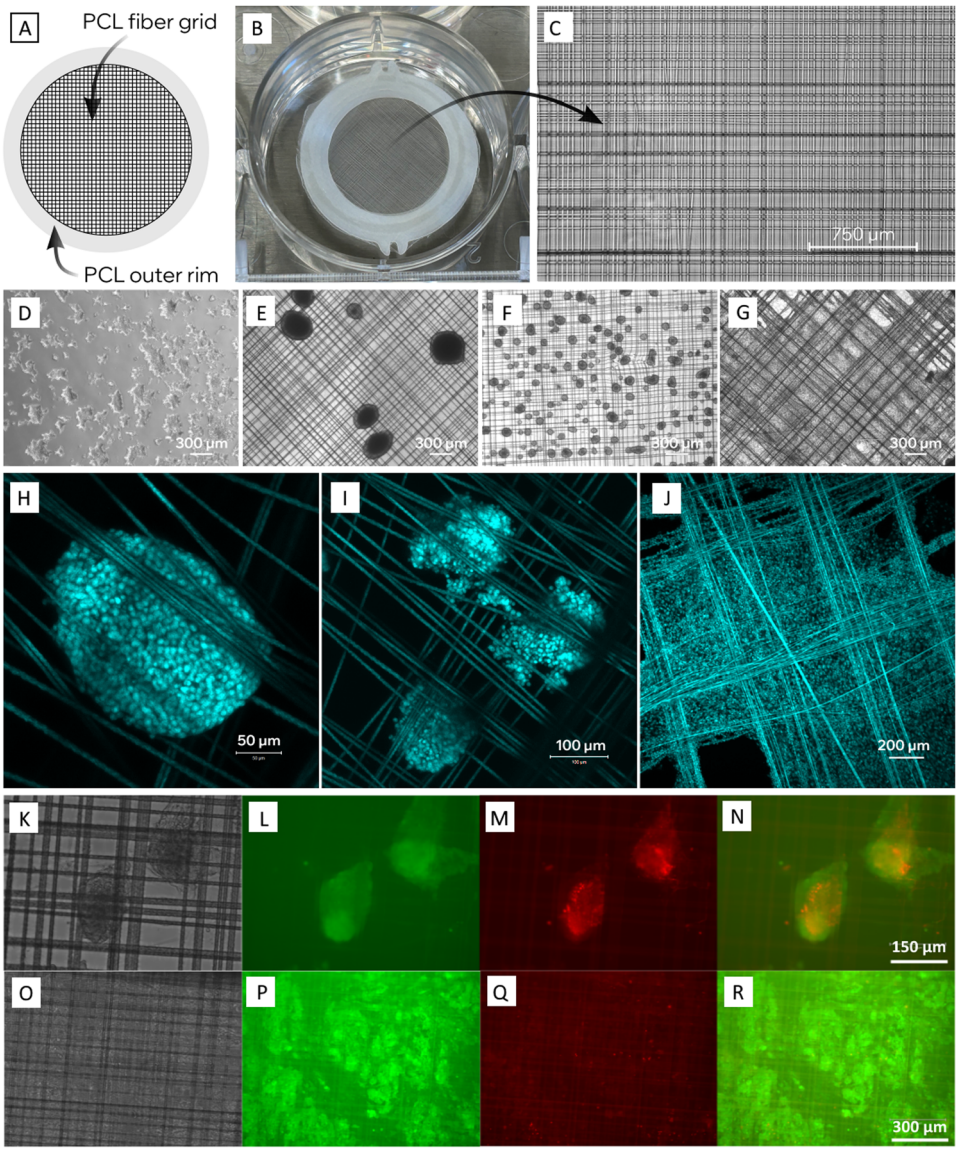

Fig. 1 Growing INS-1 cells on PCL scaffolds with and without Matrigel: (A) schematic of the scaffold; (B) a PCL scaffold in the well of a six-well plate (C) with the grid of nanofibers (scale bar = 750 μm); (D) INS-1 cells grown in a 2D culture; (E) large INS-1 spheroids on the scaffold without Matrigel; (F) small INS-1 spheroids on the scaffold with Matrigel, (G) an INS-1 cell sheet grown on the scaffold with Matrigel (scale bar = 300 μm). Confocal images of (H) INS-1 large spheroids (scale bar = 50 μm); (I) small spheroids (scale bar = 100 μm), and (J) an INS-1 cell sheet (scale bar = 200 μm). (K)–(N) Live/dead staining of INS-1 spheroids on scaffolds. (K) Bright field; (L) staining with Calcein AM (live, green); (M) staining with ethidium homodimer-1 (dead, red); (N) live/dead merged (scale bar = 150 μm). (O)–(R) Live/dead staining of an INS-1 cell sheet on scaffolds. (O) Bright field; (P) staining with calcein AM (live, green); (Q) staining with ethidium homodimer-1 (dead, red); (R) live/dead merged (scale bar = 300 μm).

pyruvate (Cat. No. TMS-005-B), 4-(2-hydroxyethyl) piperazine-1-ethanesulfonic acid (HEPES) (Cat. No. TMS-003-C), β-mercaptoethanol (Cat. No. ES-007-E), antibiotic–antimycotic (Cat. No. 15-240-112), Trypsin–EDTA (Cat. No. T4049), Dulbecco's phosphate buffered saline (DPBS) (Cat. No. D8537), Hanks' balanced salt solution (HBSS) (Cat. No. H6648), bovine serum albumin (BSA) (Cat. No. A9418), and polycaprolactone (PCL) (Cat. No. 440744, medical grade) were purchased from Millipore Sigma. 1 M Glucose (Cat. No. J60067-AK), PrestoBlue™ HS cell viability reagent (Cat. No. P50200), 4% paraformaldehyde in PBS (Cat. No. J61899.AK), and Hoechst 33342 (H3570, Invitrogen) were purchased from Thermo Fisher Scientific. Mogengel matrix organoid culture (AC-M082755), further referred to as Matrigel, was purchased from ACROBiosystems. Rodent insulin chemiluminescence ELISA (Cat. No. 80-INSMR-CH01) was purchased from American Laboratory Products Company (ALPCO).

2.1. Cell culture

The INS-1 832/13 rat insulinoma cell line was provided by CytoNest, Inc. (Athens, Ga). For culturing INS-1 cells, we prepared RPMI-1640 medium supplemented with 10% fetal bovine serum (FBS), 2 mM L-glutamine, 1 mM sodium pyruvate, 10 mM HEPES, 0.05 mM β-mercaptoethanol, and 100 units per ml of antibiotic–antimycotic. Post-thawing, the cells were plated in a

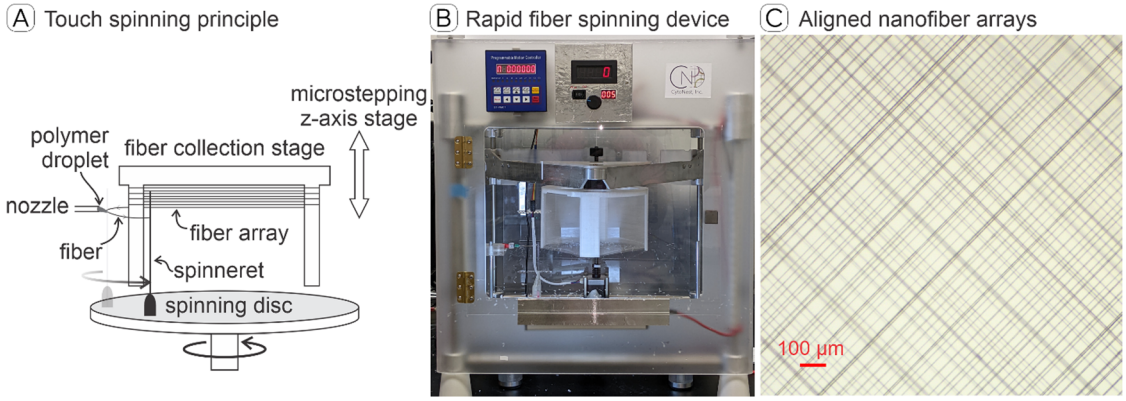

Fig. 2 Touch spinning apparatus for 3D scaffold fabrication: (A) touch spinning device concept including a spinning disc with spinneret, a polymer extrusion syringe nozzle, and a fiber collection stage; (B) touch spinning machine; (C) a PCL fiber array with crossed fibers.

T175 flask and incubated at 37 °C with 5% CO_2. Once the cells reached approximately 70% confluency, they were harvested using Trypsin–EDTA and subsequently seeded onto the scaffolds.

Additionally, NIH3T3/GFP (CMV) mouse fibroblasts, referred to as 3T3, were donated by BioAesthetics Corporation (Durham, NC). Bone marrow-derived mesenchymal stem cells (BM-MSCs) were isolated from C57BL/6J mice following the protocol outlined by Soleimani and Nadri (2009).[39] The culture medium for both 3T3s and BM-MSCs consisted of DMEM supplemented with 10% FBS and 100 units per ml of antibiotic–antimycotic.

2.2. Scaffolds

The 3D touch-spun scaffolds for cell culture were designed and fabricated at CytoNest, Inc. utilizing the touch spinning technique, as described in previous studies[37,40–44] and depicted in Fig. 2. Each scaffold is comprised of a single layer or four layers of touch-spun nanofiber mesh, with edges sealed and secured by a ring forming the outer rim or holder using a hot press (Fig. 1(A) and (B)). The fibers and the outer rim were composed of PCL, a hydrophobic material (Fig. S3) extensively employed in tissue engineering and transplantology.[45,46] The fiber mesh layer covered an area of 3.14 cm^2. The fibers were approximately 1–3 μm in diameter and were meticulously arranged in a rectangular grid, with 40–100 μm spacing between fibers.

2.3. Overlaid *vs.* fused fiber arrays

Fiber scaffolds composed of overlaid crisscross fibers, as depicted in Fig. 3(A) and (B), tend to rearrange or collapse into bundles when submerged in culture media (Fig. S2(B) and (C)). This misalignment is exacerbated during cell proliferation, creating empty gaps between cell clusters. To resolve this issue, hot air-fused PCL fiber scaffolds (Fig. 3(C) and (D)) from CytoNest, Inc. were utilized, effectively securing the fiber positions permanently both in culture media and throughout the cell proliferation process.

2.4. Seeding cells on scaffolds

Three distinct protocols (setups) for seeding INS-1 cells on scaffolds were implemented. In Setup 1, approximately one million INS-1 cells were seeded in 1 ml of media directly onto

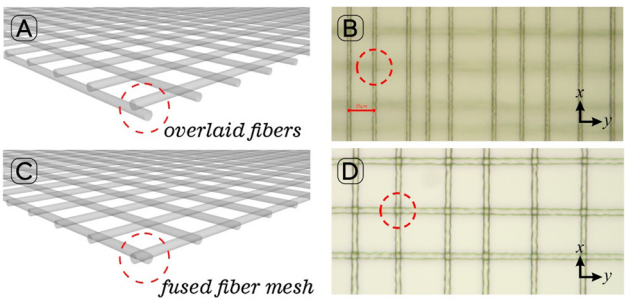

Fig. 3 Overlaid *vs.* fused PCL fiber mesh: (A) schematic of overlaid fibers in a crossed layout; (B) optical microscope image of overlaid PCL fiber array with focus on *y*-axis-oriented fibers; (C) schematic of fused fiber mesh; (D) optical microscope image of overlaid PCL fiber array with focus on *y*-axis-oriented fibers.

the scaffold without Matrigel (Fig. 4 – Setup 1). Setup 2 involved suspending approximately $2{\cdot}10^5$ cells in 1 ml of INS-1 media with 10-fold diluted Matrigel (100 μl of Matrigel in 900 μl of media). This cell/Matrigel suspension was added to single-layer scaffolds in a six-well plate containing 4 ml of media, achieving 50-fold final Matrigel dilution (Fig. 4 – Setup 2). The scaffolds were transferred to wells with fresh media without Matrigel the following day. Setup 3 involved suspending approximately $2{\cdot}10^5$ cells in 1 ml of the 10-fold diluted Matrigel. After thorough mixing, 1 ml of the suspension was applied to dry scaffolds in a six-well plate, which was then incubated at 37 °C for 30 min. Post-incubation, 4 ml of media was added (Fig. 4 – Setup 3). The scaffolds were moved to fresh media the next day. The key distinction between Setups 2 and 3 is in the manner of Matrigel application. In Setup 2, cells were initially mixed with 10-fold diluted Matrigel, while the scaffold fibers were then brought in contact with the mixture after further dilution (50-fold diluted Matrigel). In Setup 3, both cells and fibers were exposed to 10-fold diluted Matrigel for the same time.

Initially, during the cell culture period, the media was replaced every 2–3 days. However, once the cells on the scaffold achieved 50–70% confluency, the media was changed daily to accommodate increasing cellular demand.

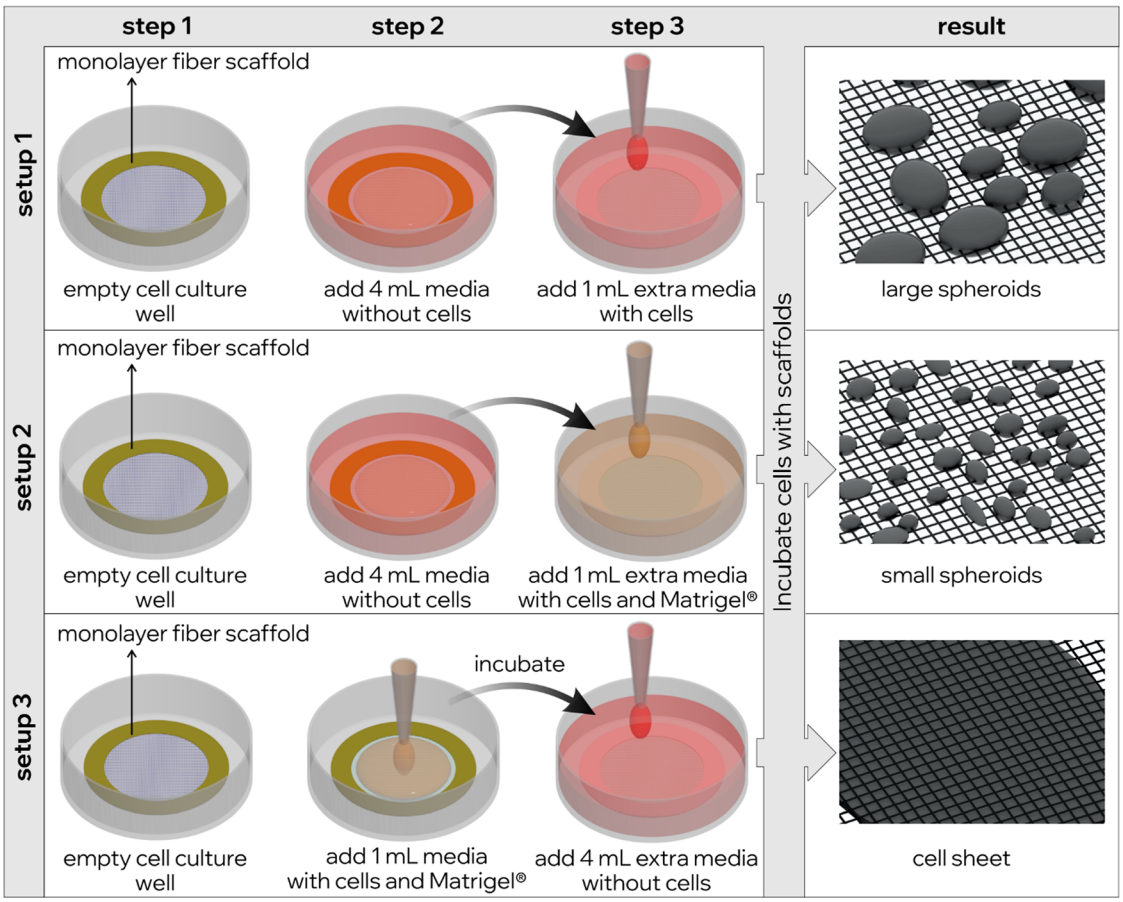

Fig. 4 Schematics of three different strategies of seeding INS-1 cells on scaffolds to obtain large spheroids (Setup 1), small spheroids (Setup 2), and cell sheets (Setup 3).

2.5. Microscopy

The growth of INS-1 cells was monitored daily with an EVOS M5000 microscope. Live/dead staining was performed with the LIVE/DEAD Viability/Cytotoxicity Kit for mammalian cells (Invitrogen, Cat. No. L3224), according to the manufacturer's instructions. For confocal microscopy analysis, the cells on the scaffolds were fixed by immersing them in 4% paraformaldehyde in DPBS at room temperature for 10 min. The fixative was subsequently removed by submerging the scaffolds in DPBS for 5 minutes. After fixation, the nuclei of the cells were stained using a 1 μg ml^{-1} Hoechst 33342 solution in DPBS. The cell cultures on the scaffolds were then imaged by placing the scaffolds in a 35-mm confocal transparent coverglass-bottom Petri dish (100350, BIOIMAGER Inc.) and using a Zeiss LSM 880 confocal microscope. After capturing the images, they were processed with ZEN software (Zeiss) for further analysis.

2.6. PrestoBlue assay

The PrestoBlue assay was conducted both before and after each glucose-stimulated insulin secretion (GSIS) test. Prior to the GSIS procedure, scaffolds with INS-1 cells were placed in wells containing 1 ml of fresh INS-1 media mixed with PrestoBlue reagent diluted at a 1 : 10 ratio. Similarly, 1 ml of this media with PrestoBlue was added to the 2D culture controls. The cells were then incubated for 2 h at 37 °C in a CO_2 incubator, after which the media was collected for absorbance measurement.

Following the GSIS test, INS-1 cells on scaffolds and in 2D cultures were rinsed with HBSS, placed in fresh media containing PrestoBlue reagent, and incubated again for 2 h at 37 °C in a CO_2 incubator. After incubation, the media was collected for absorbance analysis. The cells from the scaffolds and 2D cultures were trypsinized and counted using a Scepter 3.0 Handheld Automated Cell Counter (PHCC340KIT). To minimize the effect of detached cells on assay results, the media post-GSIS was only collected or discarded following centrifugation. Any cells collected after centrifugation were returned to their original wells with scaffolds or 2D culture.

Absorbance readings were taken at wavelengths of 570 nm and 600 nm. As a control measure, media containing a 1 : 10 dilution of PrestoBlue reagent without cells was used. The percentage reduction of PrestoBlue reagent (PRPBR) per one million cells served as an indicator of metabolic activity and was calculated using the equation provided in the manufacturer's protocol:

$$\%\ \text{Reduction of PrestoBlue reagent} = \frac{117216 \cdot A_1 - 80586 \cdot A_2}{155677 \cdot N_2 - 14652 \cdot N_1} \cdot 100$$

where A_1 is the absorbance of the test well at 570 nm, A_2 is the absorbance of the test well at 600 nm, N_1 is the absorbance of the media-only control well at 570 nm, N_2 is the absorbance of the media-only control wells at 600 nm, 117 216 is the molar extinction coefficient of oxidized Prestoblue at 600 nm, 80 586 is the molar extinction coefficient of oxidized Prestoblue at 570 nm, 155 677 is the molar extinction coefficient of reduced Prestoblue at 570 nm, and 14 652 is the molar extinction coefficient of oxidized Prestoblue at 600 nm.

Viability drop after GSIS was calculated by subtracting PRPBR after GSIS from PRPBR before GSIS. As a 2D control, we used INS-1 cells grown to confluency on the flat surface of the same area as our scaffolds (3.14 cm^2).

2.7. Glucose-stimulated insulin secretion

Prior to glucose stimulation, INS-1 cells on both scaffolds and 2D culture controls were rinsed three times with HBSS, supplemented with 0.2% bovine serum albumin (BSA) at a pH of 7.2. Subsequently, the cells on scaffolds were further washed in HBSS supplemented with 0.2% BSA and 2.5 mM glucose and then incubated in this solution for 2 h. For each well containing INS-1 cells on scaffolds and in 2D cultures, precisely 2 ml of the HBSS + BSA + glucose solution was utilized. After the 2-hour incubation period, the solution was carefully collected and stored at −80 °C for further analysis.

2.8. Insulin secretion assay

To measure concentrations of secreted insulin, we used an ALPCO Rodent Insulin Chemiluminescence ELISA kit (Cat. No. 80-INSMR-CH01). Luminescence was measured using a Biotek Synergy 2 microplate reader, using parameters described in the manufacturer's instructions. The level of the secreted insulin is presented per one million cells.

2.9. Statistical analysis

The statistical analysis was performed using the GraphPad Prism v.5 software package. The results are expressed as an arithmetic mean of at least three repeats with the standard deviation. The columns in the graphs were compared using the one-way ANOVA and the Student's *t*-test.

3. Results and discussion

It is a well-established experimental finding that different cell types demonstrate different behavior depending on the properties of their substrate.[47–49] When seeded on 3DTSS, INS-1 cells formed three-dimensional clusters resembling large (up to 1 mm in diameter) flattened spheroids (Fig. 1(H) and (I), Fig. 5A and Fig. S4), while seeded 3T3 fibroblasts formed uniform cell sheets (Fig. 6(C)). Having cells in the form of cell sheets on 3DTSS is more preferable for their future application in tissue engineering, as spheroids tend to form necrotic cores when they exceed 200 μm in size. Cell sheets rarely exceed 200 μm in thickness and hence don't form necrotic areas (Fig. 1(K)–(R)).

Another problem that we faced with INS-1 cells seeded on 3DTSS was their poor binding to the PCL fibers, compared to 3T3 fibroblasts. A one-layer scaffold is located about 1 mm above the plate bottom. After simple seeding (Fig. 4 – Setup 1), the large majority of cells fall through the scaffold between the fibers and reside on the bottom. From one million seeded cells, on average, only about 0.01% of cells were able to attach to the fibers and grow into spheroids (Fig. 7). An increase in fiber density or the addition of layers to the scaffold increased the number of attached cells (Fig. 6(A) and (B)). However, we still needed to solve this problem for non-dense, one-layered scaffolds, as our goal was to decrease the percentage of abiotic scaffold material in the entire cells/scaffold system.

We noticed no such cell adhesion problem for 3T3 (Fig. 6(C)) and BM-MSC (the image for this cell culture is not shown). This is very likely because these cell types produce a rich connective tissue-specific ECM.[50,51] To solve the problem of poor INS-1 adhesion, we enriched their ECM components by adding Matrigel. The Matrigel is a soluble form of basement membrane ECM obtained from gene-modified mouse tumor cells, mainly consisting of laminin, collagen IV, entactin, and heparin sulfate proteoglycan, and is broadly used to culture 3D organoids.[52–54] We applied Matrigel using several different methods.

The first and most straightforward approach was to deposit the undiluted Matrigel with a micropipette directly on top of a dry one-layer 3DTSS and then add the cells on top of it. The cell attachment to the fibers significantly increased, but many cells formed spheroid clumps above the scaffold and were bound to the scaffold *via* clots of undissolved Matrigel. Because of this inconvenience, this cell seeding protocol was abandoned.

Next, we tried to add Matrigel in different dilutions and combinations. As a result, we established two cell-seeding protocols (see Setups 2 and 3 in the Materials and methods section). These protocols significantly increased the number of cells attaching to fibers (Fig. 7) and completely changed the proliferation profile of INS-1 cells.

While Matrigel-free Setup 1 gives us scarce large spheroids, which can reach 350–650 μm in size on Day 23 and can grow up to 1 mm in diameter after Day 40 (Fig. 5(A)), Setup 2 resulted in the formation of numerous smaller spheroids, whose average size remained about 150 μm even by Day 23 (Fig. 5(B) and 8(A)).

When seeded following Setup 3, instead of forming spheroids, INS-1 cells grew along the fibers in the scaffolds. Initially, the cells formed flat islet-like structures, similar to those grown in 2D culture. Then, the cells blended together, forming almost uniform cell sheets (Fig. 5(C)). Imaging the INS-1 cell sheets with a confocal microscope showed that they are about 4–6 cells thick (Fig. 1(J)), which eliminates the problem of formation of the necrotic areas due to insufficient oxygen and nutrient transport (Fig. 1(K)–(R)).

Based on experimental observations, we can speculate that the structure of the Matrigel coatings on the fibers is decisive in guiding cell cluster structures. In Setup 2, cells are interacted and coated with Matrigel, which makes them more "sticky" and increases their attachment to the fibers. The reason why spheroids formed from such Matrigel-coated cells are significantly

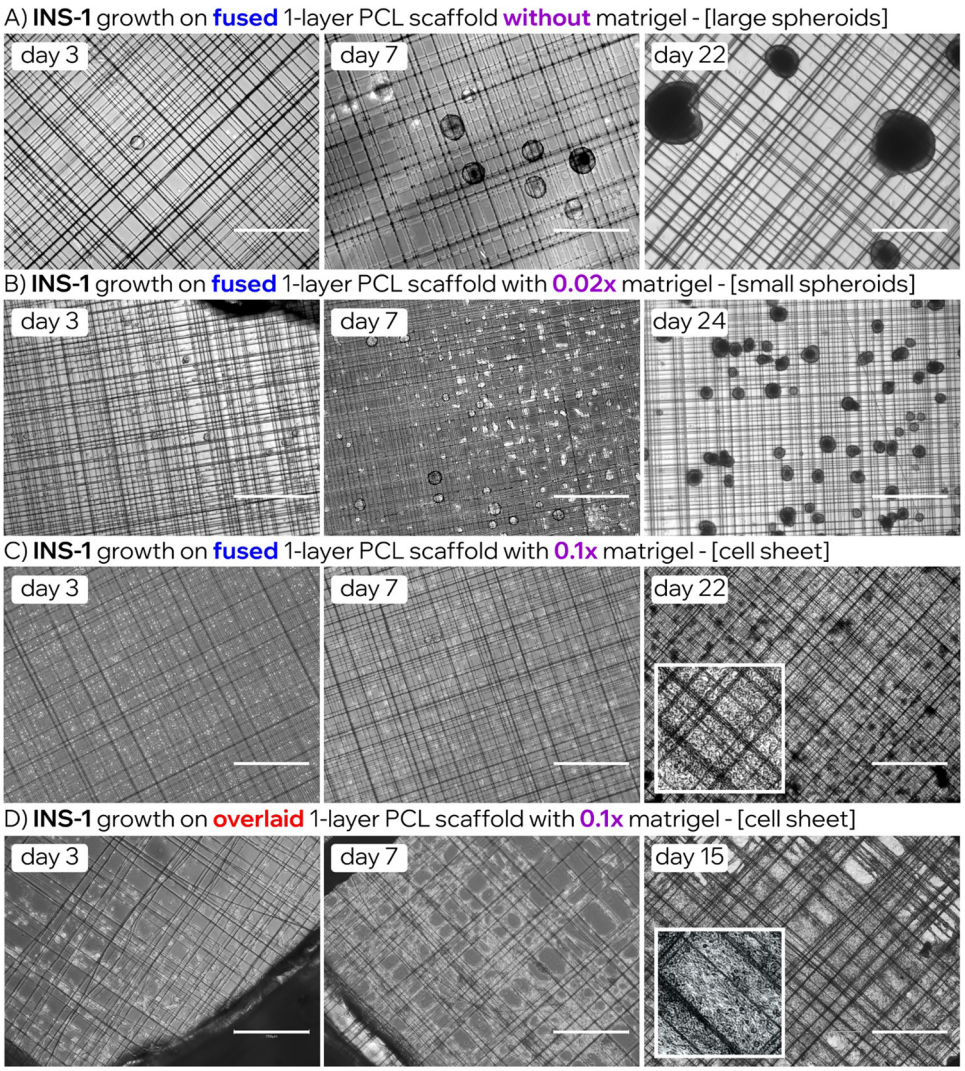

Fig. 5 INS-1 cell growth on fused/overlaid PCL 1-layer scaffolds. (A) INS-1, Protocol 1 without Matrigel results in scarce large spheroids. (B) INS-1, Protocol 2 (1 : 50 diluted Matrigel) results in small spheroids. (C) INS-1, Protocol 3 (1 : 10 diluted Matrigel) results in a cell sheet structure. (D) The experiment with non-fused fibers: INS-1, Protocol 3 (1 : 10 diluted Matrigel) results in a cell sheet structure. Scale bars = 750 μm.

smaller than Matrigel-free spheroids is unknown. Likely, a lack of ECM components in the Matrigel-free media affects cell culture development. In Setup 3, both cells and fibers are coated with Matrigel at the same dilution. As a result, more cells attached to the fibers, instead of growing on top of each other, forming spheroidal clusters. And they crawl along the fibers, using ECM-like components of Matrigel on fibers as cues to guide their movement. Thus, by growing along and around the fibers, INS-1 cells form multiple clusters that eventually fuse together due to the proximity of fibers and form cell sheet-like structures. The study of the morphology of the Matrigel coating is beyond the scope and agenda of this research. However, such a study in the future will provide important information to improve our understanding of these effects. In conclusion, adding Matrigel to 3DTSS solved two major problems: it drastically increased the number of attaching INS-1 cells and allowed them to grow as cell sheets. Growing INS-1 cells in the form of cell sheets is of utmost importance as it opens a new avenue for their use in cell sheet tissue engineering for diabetes treatment.

The fact that without Matrigel, INS-1 cells form large spheroid-like structures on 3DTSS can also have important practical applications. INS-1 3D spheroids are valuable models in early drug screening research. Still, their preparation is a very laborious procedure that requires expensive equipment (rotation system in the incubator or bioreactor) and takes up to 30 days to grow.[18] When seeded on our 3DTSS, INS-1 cells form large spheroids already by day 20, without any additional equipment (Fig. 8(A)). Besides forming large INS-1 spheroids faster than on a rotation system, changing media for spheroids bound to the scaffold is less laborious than changing media for spheroids in a suspension. Hence, 3DTSS scaffold cell culture is a competitive method to grow INS-1 spheroids.

A PrestoBlue assay was used to measure the metabolic activity and viability of the cells. The test is based on the ability of cells to metabolize resazurin (blue) into resorufin (pink). The

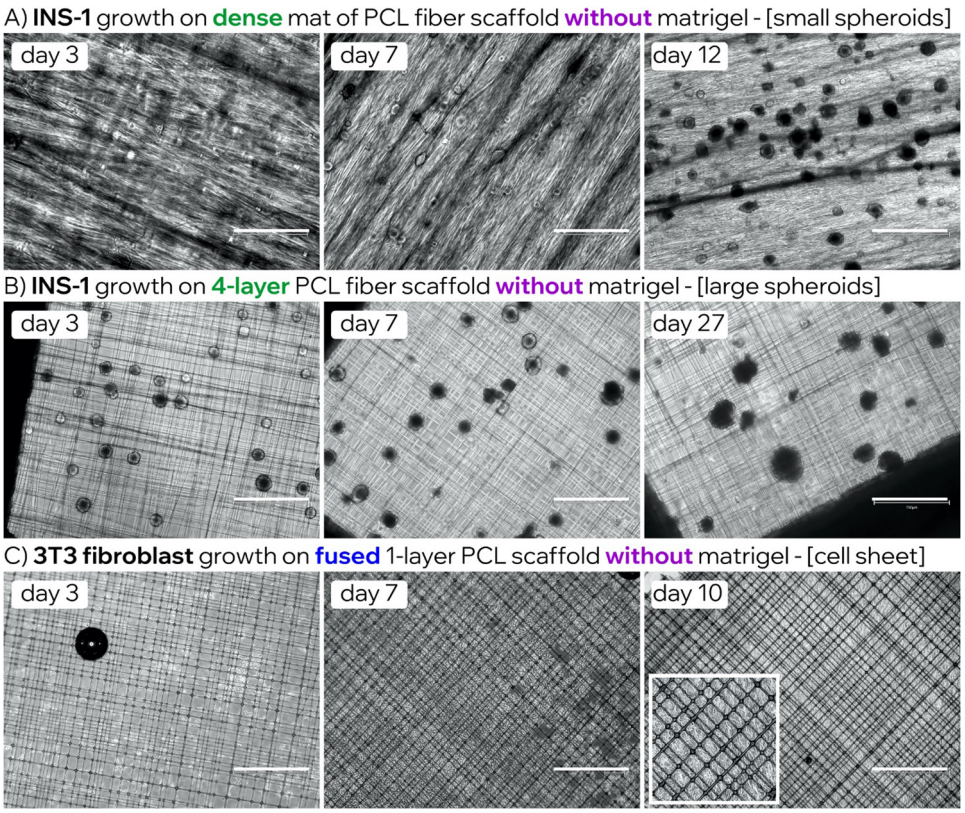

Fig. 6 Cell growth on different scaffolds. (A) INS-1 on the scaffold with densely packed fibers without Matrigel form numerous smaller spheroids. (B) INS-1 on the 4-layered scaffold with overlaid fibers without Matrigel form large spheroids. (C) 3T3 fibroblasts on 1-layered scaffold with fused fibers without Matrigel form a cell sheet structure on Day 7–10. Scale bars = 750 μm.

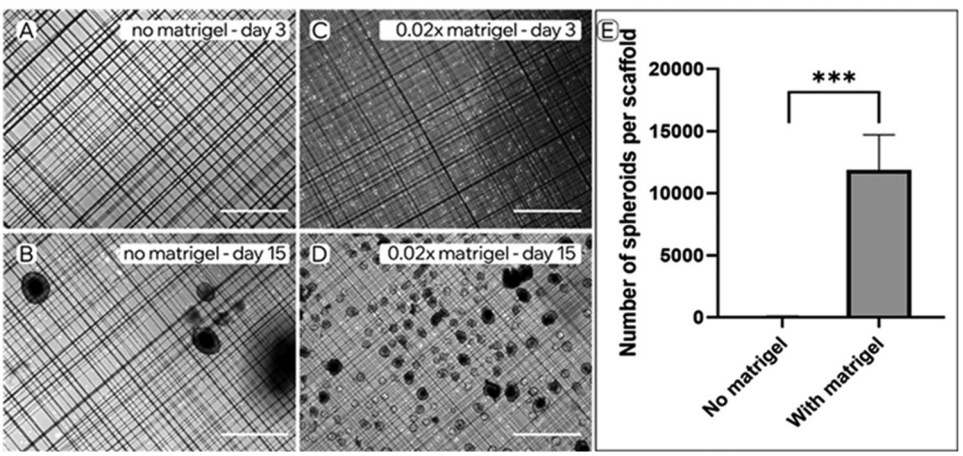

Fig. 7 The effect of Matrigel on INS-1 growth: (A) without Matrigel, 3 days after seeding; and (B) 15 days after seeding. (C) With Matrigel, 3 days after seeding, and (D) on day 15. Scale bars = 750 μm. (E) Median number of formed INS-1 spheroids on scaffolds without and with Matrigel.

results show that 2D INS-1 culture had a much higher percentage of PrestoBlue reduction compared to cell sheets and spheroids (Fig. 8(D)). However, this result is not conclusive in terms of comparing 3D and 2D cultures, as discussed in the literature.[55] The major limitation is that more cells in a 2D configuration have access to resazurin compared to clustered cells in 3D cultures. The metabolic activity of the cell sheets was close to the spheroids, which indicates that they have more in common with 3D cultures (Fig. 8(D)).

Interestingly, the cell counting after trypsinization and washing from single-layer scaffolds showed that the number of INS-1 cells in large spheroids (no Matrigel) is very similar to the number of cells in the cell sheets (with Matrigel) after the same incubation time (Fig. 8(B)). The addition of Matrigel

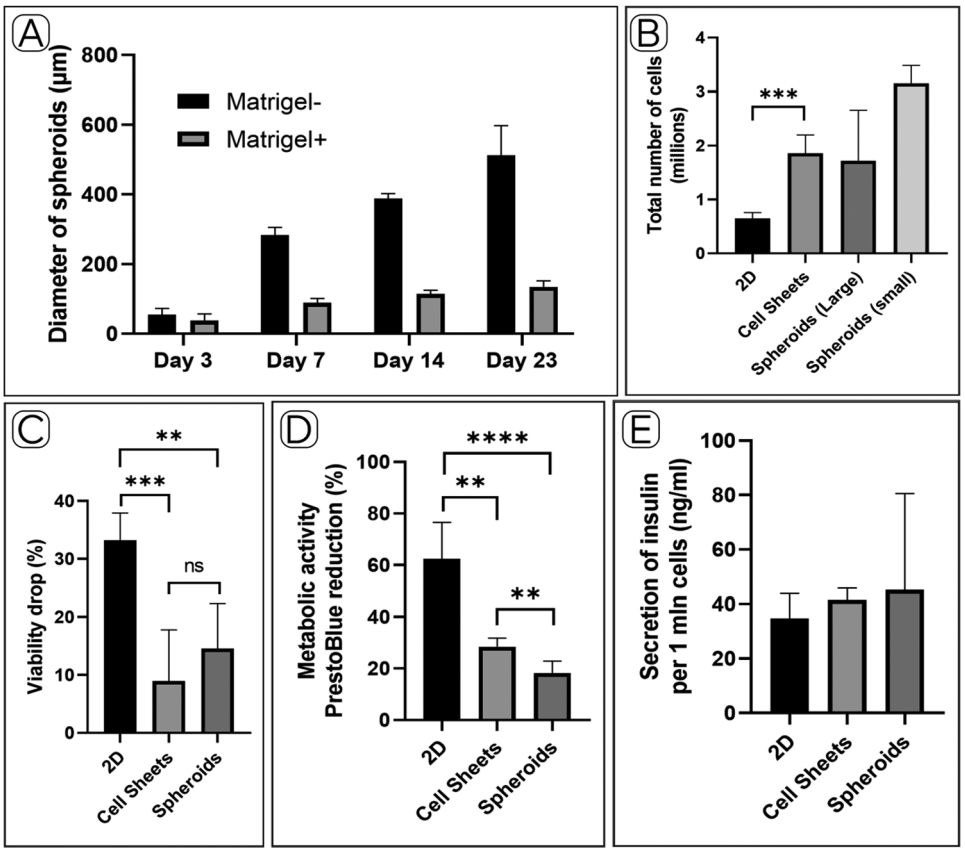

Fig. 8 Proliferation and metabolic activity of INS-1 cells grown on scaffolds as spheroids and cell sheets in comparison to 2D culture. (A) Diameter of INS-1 spheroids (median) grown on scaffolds with and without Matrigel for 23 days. (B) Number of INS-1 cells (median in millions), grown as cell sheets, large and small spheroids in comparison to 2D culture. (C) Comparison of the levels of viability after GSIS between INS-1 cells grown as 2D, cell sheets, and spheroids on scaffolds (both large and small spheroids were combined together since there was no difference between their PRPBR). (D) Comparison of PrestoBlue reagent reduction between INS-1 cells grown as 2D, cell sheets, and spheroids on scaffolds (both large and small spheroids were combined together since there was no difference between their PRPBR). (E) Secretion of insulin per one million INS-1 cells (ng ml^{-1}) grown as 2D, cell sheets, and spheroids (both large and small spheroids were combined together since there was no difference between their insulin expression).

significantly increased cell attachment, while the large spheroids grew from fewer cells, indicating that INS-1 cells in spheroids had a very good proliferation rate.

Initially, we speculated that the same number of INS-1 cells in sheets could produce more insulin than in the spheroids. This is rationalized by the fact that cells in spheroids are tightly clustered together, and the cells in the center of spheroids are less accessible to the insulin secretion stimulus (glucose). In addition, the transport of insulin from the cells closer to the center of spheroids should also be more limited. INS-1 cells in the sheet form only 4–6 cell-thick layers; consequently, they are more accessible to glucose molecules for stimulation, and delivering the secreted insulin to their environment is faster. However, the glucose stimulation with consequent ELISA assay showed that the amount of insulin produced per one million cells in 2D culture, cell sheets, and spheroids revealed no significant difference in insulin production between all the samples (Fig. 8(E)). This result is concurrent with previous findings.[18] It is likely the result of a combination of several involved mechanisms. The spheroid structure might protect the inner cells from the toxic effects of insulin accumulated in the media. Hence, glucose-stimulated cells survive longer in spheroids and produce more insulin.

The PrestoBlue viability assay on the cells before and after glucose stimulation shows that the glucose stimulation resulted in decreased cell viability (Fig. 8(C)). This can be caused by insulin-induced cell death (IICD). In the pancreas, insulin-producing β-cells are organized in highly vascularized Langerhans' islets. Due to high vascularization, the majority of secreted insulin is immediately released into the bloodstream. In the *in vitro* experiment, all secreted insulin remains in the media, which can affect cells due to its toxic effects. As was shown for chicken retina cells, insulin increases DNA fragmentation and decreases DNA synthesis in a time- and concentration-dependent manner. DNA fragmentation was increased by 92% at just 50 ng ml^{-1} insulin after 16 h of incubation.[56] In our experiments, the insulin concentration was about 100 ng ml^{-1}. It is also known that a high concentration of glucose can induce INS-1 cell/β-cell death due to oxidative stress. This phenomenon is known as high glucose-induced cell death (HGICD) or glucotoxicity.[57,58] It is possible that INS-1 could die due to a combination of IICD and HGICD. Interestingly, in our experiments, the viability drop was

more prominent in 2D culture compared to cell sheets and spheroids (Fig. 8(C)). This finding supports our hypothesis that spheroid and cell sheet clustering might protect INS-1 cells from IICD and HGICD and result in higher rates of insulin production. The exact mechanism of this phenomenon requires further studies.

As mentioned above, growing INS-1 cells on scaffolds in the form of cell sheets instead of spheroids can be very important for cell replacement therapy and *in vitro* drug testing. Using 3D spheroids and organoids for drug testing has several advantages compared to 2D cell cultures. 3D cultures have much more cell-to-cell contacts, imitating their natural environment in contrast to 2D cultures, where most contacts are between cells and the surface of the culture dish and between cells and the cell media. One of the disadvantages of spheroids and organoids *in vitro* is the formation of a necrotic core due to a lack of nutrition and oxygen when they reach 150–200 μm in diameter. INS-1 spheroids also suffer from this problem.[18] The presence of necrotic cell debris in the center of spheroids can interfere with their metabolism and can alter the results of drug testing. The presence of a necrotic core in spheroids for transplantation is also undesirable for the same reasons.

The INS-1 cell sheets are about 4–6 cells thick (Fig. 1(J)), which should eliminate the necrotic core formation (Fig. 1(K)–(R)). At the same time, they also have significantly more cell-to-cell contacts than in 2D culture because most cells grow between fibers and on top of each other. PrestoBlue assay also demonstrated that INS-1 cell sheets have metabolic activity similar to INS-1 spheroids rather than 2D culture (Fig. 8(D)). Hence, they should have all the advantages of 3D culture but no formation of necrotic areas. However, they also have several disadvantages compared to spheroids. When the confluency of the INS-1 cell sheet on the scaffold reaches 50–70%, it is necessary to change the media daily, or the cells will start to die. Interestingly, spheroids were more resilient and did not require daily media change even after reaching significant mass. Moreover, after 30 days of culturing, some INS-1 cell sheets showed signs of decline, such as massive cell loss, while INS-1 spheroids remained unchanged. All the pros and cons of using INS-1 cell sheets *vs.* INS-1 spheroids for *in vitro* research and drug testing will require further study.

Advantages of using IPCs on scaffolds for tissue engineering and cell replacement therapy include several factors. Such IPC/scaffold systems could be easy to manipulate during implantation (compared to non-fixed isolated Langerhans islets), locate, and retrieve in case of complications. A nanofiber ''skeleton'' inside the cell sheet also opens another potential application. One of the widely used scaffold-free methods in tissue engineering is the so-called cell sheet tissue engineering (CSTE). In this method, different types of cells are grown as monolayers on temperature-responsive surfaces (TRS). When TRS are cooled to room temperature, they push the layer of cells off, and the cell sheets float. These different types of cell sheets can then be sandwiched together to form a tissue-like structure.[59] Unfortunately, these cell sheets can be very thin and hard to manipulate depending on the cell type, as they easily rip, collapse, and stick together. This problem is especially relevant for IPCs, as in 2D these cells grow as separate flattened islets. On TRS they form rounded clusters that do not tend to assemble into cell sheets (Fig. S5). Since our IPC cell sheets will have rigid nanofiber ''skeletons'' inside, they are robust and can avoid all these problems. Thus, the fibrous scaffolds have potential for a scaffold-assisted CSTE method. As is known, in Type 1 diabetes, a patient's immune system is responsible for the destruction of insulin-producing β-cells, so it is very important to find a way to shield transplanted IPCs from the immune response. A CSTE technique might be useful to create such natural ''shields'' for IPCs from layers of immune-privileged cells, such as BM-MSCs or Sertoli cells (Fig. S2(A)). Additionally, since 3DTSS/cell sheets utilize significantly less scaffold material, the scaffold components will be resorbed considerably faster than, for instance, denser electrospun or 3D-printed scaffolds (Table 1).

Future studies will also need to determine if IPC in the form of spheroids or cell sheets has more advantages for transplantation. Theoretically, IPC sheets on scaffolds, being only 4–6 cells thick, would not require immediate vascularization to survive as they can draw enough nutrients and oxygen from the surrounding tissues. Spheroids, on the other hand, without fast vascularization, might start forming necrotic cores upon reaching 150–200 μm thickness. However, INS-1 spheroids showed a tendency for higher preservation of their viability after glucose stimulation (Fig. 8(c)). Besides that, multiple spheroids on scaffolds can contain more cells (Fig. 8B) and produce more insulin. IPCs in spheroids visibly look sturdier; the cells should have fewer chances to break away and migrate to other parts of the body. This is compared to cell sheets on scaffolds, where large chunks of cells hang between fibers and can break away during rough manipulations. Another problem related to using Matrigel on scaffolds is that Matrigel batches have a variable composition, which might lead to inconsistent results and troubles with reproducibility.[60–62] Future *in vivo* experiments will help to determine all the pros and cons of IPC cell sheets/scaffolds *vs.* spheroids/scaffolds for cell replacement therapy.

4. Conclusions

We applied innovative touch-spun three-dimensional fibrous scaffolds made of fused fiber meshes that enable the growth of adherent cell cultures in 3D, mimicking tissue-like structures. These scaffolds are optimized for enhanced space and uniform cell adhesion to achieve cell confluency in 3D. We found that adding Matrigel to 3DTSS significantly enhances cell attachment and enables us to modify the proliferation profile of INS-1 cells in a concentration-dependent manner. We devised three cell-seeding protocols to grow INS-1 cells on 3DTSS in different forms: large spheroids, small spheroids, and cell sheets.

All three forms of INS-1 on 3DTSS and INS-1 cells in 2D culture displayed comparable levels of secreted insulin. These qualities make INS-1 small spheroids and cell sheets on 3DTSS attractive models for *in vitro* research and drug testing, and they show great potential for creating insulin-producing implants for diabetes treatment and management.

Both small INS-1 spheroids and cell sheets, due to their small size/thickness, are less prone to the necrotic core than large spheroids. INS-1 cell sheets have a metabolic profile similar to spheroids and exhibit many cell-to-cell contacts. Further studies are needed to assess all the advantages and disadvantages of using INS-1 spheroids *versus* INS-1 cell sheets in both *in vitro* research and *in vivo* cell replacement therapy.

Author contributions

M. Parker: investigation, methodology, writing; N. S. Yadavalli: conceptualization, methodology, writing – review; K. Peranidze: investigation; E. Boland: methodology, writing – review; V. Reukov: methodology, writing – review; S. Minko: conceptualization, methodology, writing – review & editing.

Conflicts of interest

NSY and SM are co-founders of the CytoNest startup.

Data availability

All data generated or analyzed during this study are included in this published article.

Supplementary information: This supplementary data complements the main manuscript by providing images for comparison of the touch-spun and electrospun scaffolds, cells on fibrous scaffolds and 2D susbstates, surface wetting, and a combination of cell sheets. See DOI: **https://doi.org/10.1039/d5tb00519a**

Acknowledgements

This research was supported by the Georgia Research Alliance (grant title: BioScaffold: Nanofiber 3D Scaffolding Devices for 3D Cell Culture). NSY and SM acknowledge the awards of the USDA National Institute of Food and Agriculture STTR Program, USA (grant number: 2023-51402-39329) and the Good Food Institute for the support of 3D scaffold development (grant title: Tailored, Edible, and Scalable 3D Fiber Scaffolds for Shrimp Cell Expansion).

References

1 G. A. Gregory, T. I. G. Robinson, S. E. Linklater, F. Wang, S. Colagiuri, C. de Beaufort, K. C. Donaghue, International Diabetes Federation Diabetes Atlas Type 1 Diabetes in Adults Special Interest Group, D. J. Magliano, J. Maniam, T. J. Orchard, P. Rai and G. D. Ogle, *Lancet Diabetes Endocrinol.*, 2022, **10**, 741.
2 Z. Czarnecka, N. Dadheech, H. Razavy, R. Pawlick and A. M. J. Shapiro, *Cells*, 2023, **12**, 2423.
3 D. J. Holmes-Walker, J. E. Gunton, W. Hawthorne, M. Payk, P. Anderson, S. Donath, T. Loudovaris, G. M. Ward, T. W. Kay and P. J. O'Connell, *Transplantation*, 2017, **101**, 1268.
4 A. J. Shapiro, J. R. Lakey, E. A. Ryan, G. S. Korbutt, E. Toth, G. L. Warnock, N. M. Kneteman and R. V. Rajotte, *N. Engl. J. Med.*, 2000, **343**, 230.
5 A. J. Shapiro, C. Ricordi, B. J. Hering, H. Auchincloss, R. Lindblad, R. P. Robertson, A. Secchi, M. D. Brendel, T. Berney and D. C. Brennan, *N. Engl. J. Med.*, 2006, **355**, 1318.
6 K. E. Kador and J. L. Goldberg, *Expert Rev. Ophthalmol.*, 2012, **7**, 459.
7 K. G. Maxwell and J. R. Millman, *Cell Rep. Med.*, 2021, **2**, 100238.
8 S. Pellegrini, V. Zamarian, E. Landi, A. Cospito, M. T. Lombardo, F. Manenti, A. Citro, M. Schiavo Lena, L. Piemonti and V. Sordi, *Int. J. Mol. Sci.*, 2022, **23**, 9699.
9 S. Pellegrini, V. Zamarian and V. Sordi, *Transpl. Int.*, 2022, **35**, 10575.
10 A. De Pieri, Y. Rochev and D. I. Zeugolis, *npj Regener. Med.*, 2021, **6**, 18.
11 Q. Dang Le, W. Rodprasert, S. Kuncorojakti, P. Pavasant, T. Osathanon and C. Sawangmake, *Sci. Rep.*, 2022, **12**, 9127.
12 D. W. Clough, J. L. King, F. Li and L. D. Shea, *Endocrinology*, 2020, **161**(11), bqaa156.
13 G. A. Salg, N. A. Giese, M. Schenk, F. J. Hüttner, K. Felix, P. Probst, M. K. Diener, T. Hackert and H. G. Kenngott, *J. Tissue Eng.*, 2019, **10**, 2041731419884708.
14 G. Christoffersson, *J. Immunol. Regener. Med.*, 2022, **15**, 100057.
15 I. B. B. Silva, C. H. Kimura, V. P. Colantoni and M. C. Sogayar, *Stem Cell Res. Ther.*, 2022, **13**, 309.
16 C. Yun, S. H. Kim, K. M. Kim, M. H. Yang, M. R. Byun, J. H. Kim, D. Kwon, H. T. M. Pham, H. S. Kim, J. H. Kim and Y. S. Jung, *Int. J. Mol. Sci.*, 2024, **25**, 2512.
17 N.-E. Ryu, S.-H. Lee and H. Park, *Cells*, 2019, **8**, 1620.
18 Y. Ntamo, E. Samodien, J. Burger, N. Muller, C. J. Muller and N. Chellan, *Front. Cell Dev. Biol.*, 2021, **8**, 623889.
19 K. Białkowska, P. Komorowski, M. Bryszewska and K. Miłowska, *Int. J. Mol. Sci.*, 2020, **21**, 6225.
20 S. Lagies, M. Schlimpert, S. Neumann, A. Wäldin, B. Kammerer, C. Borner and L. Peintner, *Commun. Biol.*, 2020, **3**, 246.
21 K. Sharma, S. Dey, R. Karmakar and A. K. Rengan, *Cancer Innovation.*, 2024, **3**, e102.
22 M. P. Nikolova and M. S. Chavali, *Bioact. Mater.*, 2019, **4**, 271.
23 L. Bačáková, K. Novotná and M. Pařízek, *Physiol. Res.*, 2014, **63**, S29.
24 T. Paramasivam, S. K. Maiti, S. Palakkara, Rashmi, D. Mohan, H. V. Manjunthaachar, K. Karthik and N. Kumar, *Tissue Eng. Regener. Med.*, 2021, **18**, 235.
25 H. Y. Lin, H. H. Chen, S. H. Chang and T. S. Ni, *J. Biomater. Sci., Polym. Ed.*, 2013, **24**, 470.
26 X. J. Li, A. V. Valadez, P. Zuo and Z. Nie, *Bioanalysis*, 2012, **4**, 1509.
27 W. H. Abuwatfa, W. G. Pitt and G. A. Husseini, *J. Biomed. Sci.*, 2024, **31**, 7.
28 N. Abdul Kareem, A. Aijaz and M. G. Jeschke, *Biologics*, 2021, **15**, 379.
29 I. Jun, H. S. Han, J. R. Edwards and H. Jeon, *Int. J. Mol. Sci.*, 2018, **19**, 745.

30 B. N. Blackstone, A. F. Palmer, H. R. Rilo and H. M. Powell, *Tissue Eng., Part A*, 2014, **20**, 1784.
31 R. Scharfmann, W. Staels and O. Albagli, *J. Clin. Invest.*, 2019, **129**, 3511.
32 M. Barisam, M. S. Saidi, N. Kashaninejad and N. T. Nguyen, *Micromachines*, 2018, **9**, 94.
33 R. K. Jain, P. Au, J. Tam, D. G. Duda and D. Fukumura, *Nat. Biotechnol.*, 2005, **23**, 821.
34 M. Asfari, D. Janjic, P. Meda, G. Li, P. A. Halban and C. B. Wollheim, *Endocrinology*, 1992, **130**, 167.
35 J. Lang, M. Fukuda, H. Zhang, K. Mikoshiba and C. B. Wollheim, *EMBO J.*, 1997, **16**, 5837–5846.
36 H. E. Hohmeier, H. Mulder, G. Chen, R. Henkel-Rieger, M. Prentki and C. B. Newgard, *Diabetes*, 2000, **49**, 424.
37 D. Asheghali, S.-J. Lee, A. Furchner, A. Gruzd, S. Larson, A. Tokarev, S. Stake, X. Zhou, K. Hinrichs and L. G. Zhang, *Nanomedicine*, 2020, **24**, 102152.
38 S.-J. Lee, D. Asheghali, B. Blevins, R. Timsina, T. Esworthy, X. Zhou, H. Cui, S. Y. Hann, X. Qiu and A. Tokarev, *ACS Appl. Mater. Interfaces*, 2019, **12**, 2067.
39 M. Soleimani and S. Nadri, *Nat. Protoc.*, 2009, **4**, 102.
40 S.-J. Lee, D. Asheghali, B. Blevins, R. Timsina, T. Esworthy, X. Zhou, H. Cui, S. Y. Hann, X. Qiu, A. Tokarev, S. Minko and L. G. Zhang, *ACS Appl. Mater. Interfaces*, 2020, **12**, 2067.
41 A. Tokarev, D. Asheghali, I. M. Griffiths, O. Trotsenko, A. Gruzd, X. Lin, H. A. Stone and S. Minko, *Adv. Mater.*, 2015, **27**, 6526.
42 K. Hinrichs, B. Blevins, A. Furchner, N. S. Yadavalli and S. Minko, *Micro Nano Eng.*, 2022, **14**, 100116.
43 D. Asheghali, S.-J. Lee, A. Furchner, A. Gruzd, S. Larson, A. Tokarev, S. Stake, X. Zhou, K. Hinrichs, L. G. Zhang and S. Minko, *Nanomedicine*, 2020, **24**, 102152.
44 H. Gao, D. Asheghali, N. S. Yadavalli, M. T. Pham, T. D. Nguyen, S. Minko and S. Sharma, *J. Text. Inst.*, 2020, **111**, 906.
45 Q. Chen, S. Liang and G. A. Thouas, *Prog. Polym. Sci.*, 2013, **38**, 584.
46 A. M. Coenen, K. V. Bernaerts, J. A. Harings, S. Jockenhoevel and S. Ghazanfari, *Acta Biomater.*, 2018, **79**, 60.
47 H. Amani, H. Arzaghi, M. Bayandori, A. S. Dezfuli, H. Pazoki-Toroudi, A. Shafiee and L. Moradi, *Adv. Mater. Interfaces*, 2019, **6**, 1900572.
48 S. Cai, C. Wu, W. Yang, W. Liang, H. Yu and L. Liu, *Nanotechnol. Rev.*, 2020, **9**, 971.
49 B. Majhy, P. Priyadarshini and A. Sen, *RSC Adv.*, 2021, **11**, 1546.
50 R. T. Kendall and C. A. Feghali-Bostwick, *Front. Pharmacol.*, 2014, **5**, 123.
51 M. Marinkovic, O. N. Tran, T. J. Block, R. Rakian, A. O. Gonzalez, D. D. Dean, C.-K. Yeh and X.-D. Chen, *Matrix Biol. Plus*, 2020, **8**, 100044.
52 J. H. Heo, D. Kang, S. J. Seo and Y. Jin, *Int. J. Stem Cells*, 2022, **15**, 60.
53 N. Georgakopoulos, N. Prior, B. Angres, G. Mastrogiovanni, A. Cagan, D. Harrison, C. J. Hindley, R. Arnes-Benito, S.-S. Liau and A. Curd, *BMC Dev. Biol.*, 2020, **20**, 1.
54 D. Dutta, I. Heo and H. Clevers, *Trends Mol. Med.*, 2017, **23**, 393.
55 P. S. Thakuri, M. Gupta, M. Plaster and H. Tavana, *Assay Drug Dev. Technol.*, 2019, **17**, 140.
56 G. Calvaruso, R. Vento, E. Gerbino, M. Lauricella, M. Carabillò, H. Main and G. Tesoriere, *Cell Death Differ.*, 1997, **4**, 209.
57 S. Lablanche, C. Cottet-Rousselle, F. Lamarche, P.-Y. Benhamou, S. Halimi, X. Leverve and E. Fontaine, *Cell Death Dis.*, 2011, **2**, e134.
58 W.-H. Kim, J. W. Lee, Y. H. Suh, S. H. Hong, J. S. Choi, J. H. Lim, J. H. Song, B. Gao and M. H. Jung, *Diabetes*, 2005, **54**, 2602.
59 P. Thummarati, W. Laiwattanapaisal, R. Nitta, M. Fukuda, A. Hassametto and M. Kino-Oka, *Bioengineering*, 2023, **10**, 211.
60 E. Lingard, S. Dong, A. Hoyle, E. Appleton, A. Hales, E. Skaria, C. Lawless, I. Taylor-Hearn, S. Saadati and Q. Chu, *Biomater. Adv.*, 2024, **160**, 213847.
61 E. A. Aisenbrey and W. L. Murphy, *Nat. Rev. Mater.*, 2020, **5**, 539.
62 S. Kaur, I. Kaur, P. Rawal, D. M. Tripathi and A. Vasudevan, *Cancer Lett.*, 2021, **504**, 58.